Rapid Communications

Discrete propagation of trapped modes in acoustic waveguide arrays

Miguel Molerón*
Institute of Geophysics, Department of Earth Sciences, Swiss Federal Institute of Technology (ETH Zurich) Zurich, Sonneggstrasse 5, 8092 Zurich, Switzerland

Cédric Faure, Simon Félix, Vincent Pagneux, and Olivier Richoux
Laboratoire d'Acoustique de l'Université du Mans (LAUM) - CNRS UMR 6613, Avenue Olivier Messiaen, 72085 Le Mans, France

(Received 19 June 2018; revised manuscript received 21 November 2018; published 6 May 2019)

Arrays of evanescently coupled waveguides in which wave behavior becomes discretized exhibit unique wave dynamics, and they offer the possibility to investigate analogous fundamental quantum phenomena at accessible time and length scales. In this Rapid Communication, we investigate the discretelike propagation of trapped modes in airborne acoustic waveguide arrays. Using numerical simulations and experiments, we analyze the emergence of acoustic discrete diffraction and spatial Bloch oscillations in the array. Furthermore, exploiting the Bloch oscillations phenomenon, we demonstrate the possibility to generate diffraction-free acoustic beams and to focus the acoustic energy within a single lattice site at distances orders of magnitude larger than the operating wavelength.

DOI: 10.1103/PhysRevB.99.201404

Light propagating in arrays of evanescently coupled waveguides exhibits behavior that is characteristic of discrete media [1,2]. This feature gives rise to a number of phenomena that are not accessible in continuous media, such as discrete diffraction, diffraction management [3,4], or discrete solitons [5,6], with great potential for engineering applications [1,2]. Another interesting feature of waveguide arrays is that the spatial evolution of the optical field in the array is analogous to the time evolution of the probability function of an electron in a tight-binding lattice [7,8]. Thus, waveguide arrays constitute a versatile test bed in which analogous quantum mechanical effects can be investigated at easily observable time and length scales. This includes quantum walks [9–11], Bloch oscillations (BOs) [12–15], dynamic localization [16,17], and more (see Ref. [18] for a detailed review).

Extending these ideas to airborne acoustics is of great interest for several reasons. As shown in this Rapid Communication, the unique dynamical properties of waveguide arrays give us entirely different possibilities to manipulate acoustic waves. In addition, airborne acoustic waveguide arrays (AWAs) allow for an easy measurement and input phase control of individual waveguides, making AWAs a versatile platform for investigating discretelike wave propagation phenomena. However, very few studies have investigated discretelike wave propagation in AWAs. For instance, Ye *et al.* [19] demonstrated Anderson localization in AWAs with random couplings between adjacent guides. However, this work was limited to the fundamental plane mode associated with rigid walls (i.e., with Neumann boundary conditions); indeed, the phase velocity of this planar mode is always the free-space phase velocity and it is independent from the transverse geometry structure. This hinders the implementation of other discretelike phenomena linked to the lateral modulation of the propagation constant. In this Rapid Communication, we investigate theoretically and experimentally AWAs that support an antisymmetric trapped mode (with respect to the midplane of the array) with a propagation constant that can be straightforwardly adjusted with the waveguide height. Taking advantage of this property, we study the emergence of spatial BOs in the array when a linear gradient of the propagation constant is applied. In addition, the trapped nature of the antisymmetric mode makes it possible to manipulate acoustic waves at very long distances. We exploit this feature to demonstrate the formation of diffraction-free acoustic beams and subwavelength focusing at distances orders of magnitude larger than the free-space operating wavelength. Acoustic BOs have been demonstrated in several setups [20–28]. An experimental demonstration of spatial BOs for airborne sound is shown in this Rapid Communication.

The system under consideration is illustrated in Fig. 1(a). The array is symmetric with respect to the the xz midplane and it is composed of N coupled waveguides with a rectangular cross section with dimensions $L \times H_n$, where n indicates the lattice site, $n = 1, 2, \ldots, N$. The waveguides are connected via a narrow coupling region with dimensions $l \times h_n$, and $d = L + l$ denotes the period of the array. The waveguides are infinite and homogenous in the z direction and all boundaries are considered as perfectly rigid.

The symmetric cross section makes two independent modal families appear: symmetric modes and antisymmetric modes with respect to the x axis. For a single, uncoupled waveguide the propagation constants of these modes are $\beta_n^{\mu,\nu} = \sqrt{(\frac{\omega}{c})^2 - (\alpha_n^{\mu,\nu})^2}$, where ω is the angular frequency, c is the sound speed in air, and $\alpha_n^{\mu,\nu} = \pi\sqrt{(\mu/L)^2 + (\nu/H_n)^2}$ is the wave number in the xy plane, where $\mu, \nu \in \mathbb{N}$ indicate,

*miguel.moleron@gmail.com

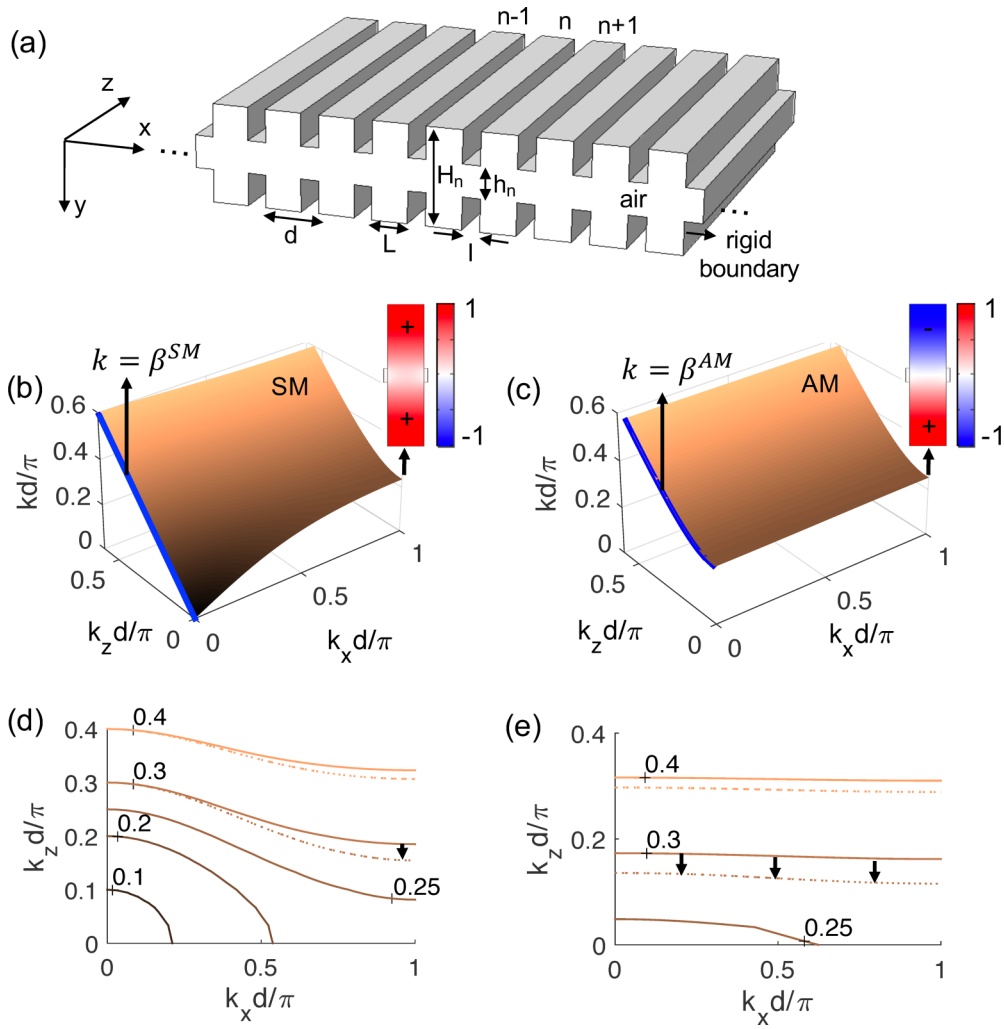

FIG. 1. (a) Schematic of the AWA. The array is infinite in the propagation direction z and has a symmetric cross section with respect to the x axis. H_n is the height of waveguide n, L is the waveguide width, h_n is the height of the coupling region between waveguides n and $n+1$, l is the separation distance between two adjacent guides, and $d = L + l$ is the period of the AWA. (b) and (c) show, respectively, the dispersion relation of the SM and the AM for a homogeneous array with dimensions $H_n = d/0.24$, $h_n = d/1.6$, $L = d/1.2$, and $l = d/6$. The inset shows the normalized SM and AM at the resonance frequency ($kd/\pi = 0.236$ for the SM and $kd/\pi = 0.252$ for the AM). The thick blue line in the plane $k_x = 0$ represents the dispersion relation of the SM and AM of an uncoupled waveguide. (d) and (e) Isofrequency contours of the SM and AM, respectively. The dashed lines in (d) and (e) represent the isofrequency contours of a similar array, except that the waveguide height is 8% smaller.

respectively, the number of vertical and horizontal nodal lines. ν determines the symmetry of the mode: ν is even for symmetric modes and odd for antisymmetric modes. Since we are interested in the regime in which only one mode of each family propagates, we restrict our analysis to the first symmetric and antisymmetric modes, hereafter referred to as SM and AM, with propagation constants $\beta_n^{\mathrm{SM}} = \beta_n^{0,0} = \omega/c$ and $\beta_n^{\mathrm{AM}} = \beta_n^{0,1} = \sqrt{(\frac{\omega}{c})^2 - (\frac{\pi}{H_n})^2}$.

First, we analyze the discrete diffraction phenomenon in a homogeneous array with dimensions $H_n = d/0.24$, $h_n = d/1.6$, $L = d/1.2$, and $l = d/6$. The choice of these parameters is explained in Ref. [29]. The key physical ingredient that enables discrete diffraction is the evanescent coupling between adjacent waveguides [3]. To find out the frequency range in which this occurs, we have computed, using COMSOL MULTIPHYSICS, the SM and AM dispersion relations, shown in Figs. 1(b) and 1(c). The dispersion in the z direction coincides with the propagation constants of the uncoupled, individual waveguides, as indicated by the solid blue lines in the plane $k_x = 0$. However, in the x direction, the dispersion relation of both the SM and AM is dominated by a resonance of the upper and lower cavities forming the waveguides. The cavities resonate in phase for the SM and out of phase for the AM [see the insets in Figs. 1(b) and 1(c)]. This resonance creates a band gap in the x direction starting at frequencies $kd/\pi = 0.236$ for the SM and $kd/\pi = 0.252$ for the AM.

Figures 1(d) and 1(e) show, respectively, isofrequency contours of the dispersion relation at several frequencies. Below the resonance, the array behaves as an anisotropic bulk medium, with elliptic isofrequency contours intersecting the k_x axis. However, above the resonance, the isofrequency contours no longer intersect the k_x axis. This indicates an

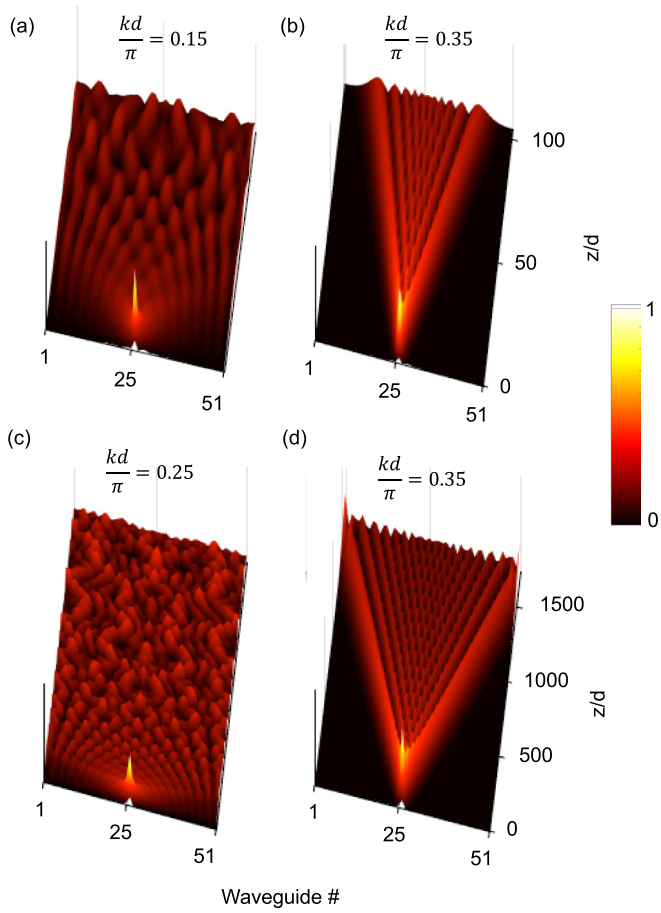

FIG. 2. (a) Symmetric part of the pressure field at $kd/\pi = 0.15$, (b) symmetric part of the pressure field at $kd/\pi = 0.35$, (c) antisymmetric part of the pressure field at frequency $kd/\pi = 0.25$, and (c) antisymmetric part of the pressure field at frequency $kd/\pi = 035$.

evanescent coupling in the x direction that leads to discrete diffraction [3].

To visualize the continuous and discrete propagation regimes, Fig. 2 displays the magnitude of the symmetric and antisymmetric parts of the pressure field when a finite homogenous array composed of $N = 51$ waveguides is excited at frequencies below [Figs. 2(a) and 2(c)] and above [Figs. 2(b) and 2(d)] the resonance frequency. The pressure field was computed using the modal-finite-element (FE) method. This method calculates the eigenmodes of the whole cross section of the array (supermodes) using finite elements and uses a multimodal formulation to compute the propagation in the z direction (see Refs. [29–32]). As a source, we used a Gaussian beam located at the center of waveguide $n = 26$ at height $y = H_n/4$, in order to excite symmetric and antisymmetric supermodes.

Below the resonance [Figs. 2(a) and 2(c)] the field spreads rapidly in the lateral direction due to the coupling of the initial excitation with propagative waves in x. The interference pattern observed in this case is due to multiple wave reflections on the lateral boundaries of the array. However, at frequencies in the band gap [Figs. 2(b) and 2(d)], one observes a much slower spreading in the lateral direction due to the evanescent coupling in x. In this regime, the field exhibits a characteristic discrete diffraction pattern with two high amplitude side lobes and an interference pattern in the middle, resulting from the constructive and destructive interference of waves hopping between adjacent waveguides. This field evolution is analogous to the quantum random walk of a localized particle in a tight-binding lattice [33], and it is at the origin of diffraction management in optical waveguide arrays [3].

Figure 2 shows that the propagation of both the SM and AM becomes discretized at frequencies in the band gap. However, a remarkable difference of the AM with respect to the SM is the extreme flatness of its isofrequency contours, which is due to the trapped nature of the AM (see Refs. [34–36] for more details). As a consequence, the spreading angle of the AM is considerably narrower than that of the SM [note the difference in the length scales between Figs. 2(b) and 2(d)]. This property gives us the possibility to manipulate acoustic waves at very long distances. Furthermore, as stated above, we see that the dispersion relation of the SM in the z direction (plane mode) is fixed to $k(k_x = 0) = \beta^{\mathrm{SM}}$, i.e., it is independent from the transverse geometry. This is in contrast with the AM, whose dispersion relation can be fully controlled with the waveguide height. This is illustrated in Figs. 1(d) and 1(e), where dashed lines represent the isofrequency contours of a similar array but with a waveguide height 8% smaller than in the previous case. While the SM isofrequency contours remain fixed at $k_x = 0$, the AM isofrequency contours are downshifted for all values of k_x. In the following, we use this property to investigate the formation of spatial BOs when a constant spacing of the propagation constant $\Delta\beta$ is created through a varying height profile. The detailed derivation of the height profile is given in Ref. [29].

In the framework of waveguide arrays, the constant spacing $\Delta\beta$ plays the role of a constant force applied on a particle in a periodic potential, which is responsible for electronic Bloch oscillations [13,37]. Figures 3(a)–3(d) display, respectively, the antisymmetric part of the acoustic field for a Gaussian beam width of $\sigma = 0.17d$, $0.83d$, $1.67d$, and $3.33d$, at frequency $kd/\pi = 0.35$. When the excitation is very narrow compared to d [i.e., a single waveguide is excited, Fig. 3(a)], the field spreads in the array following a discrete diffraction pattern similar to that observed in Fig. 2(d). However, unlike in the homogeneous array, the energy refocuses completely within a single lattice site at a distance equal to the Bloch oscillation period $L_B = 2\pi/\Delta\beta$. As the excitation width increases [see Figs. 3(b)–3(d)] the acoustic field evolves to an oscillatory motion in which the wave packet moves periodically in the x direction, but keeping a constant width. The periodic recurrence of the acoustic field in the array is a consequence of the so-called Wannier-Stark ladders, a series of antisymmetric supermodes with equidistant propagation constants (see Ref. [29] for details).

The existence of BOs in the array gives us access to remarkable wave dynamical properties. Besides the formation of diffraction-free acoustic beams in Fig. 3(d), Fig. 3(a) shows the possibility to confine laterally the acoustic energy in a subwavelength region at a distance L_B arbitrarily larger than the free-space operational wavelength λ. This is an important issue both from fundamental and technological points of view [38–40]. This can be achieved by selecting a lattice constant d (or focal spot) much smaller than λ. In the

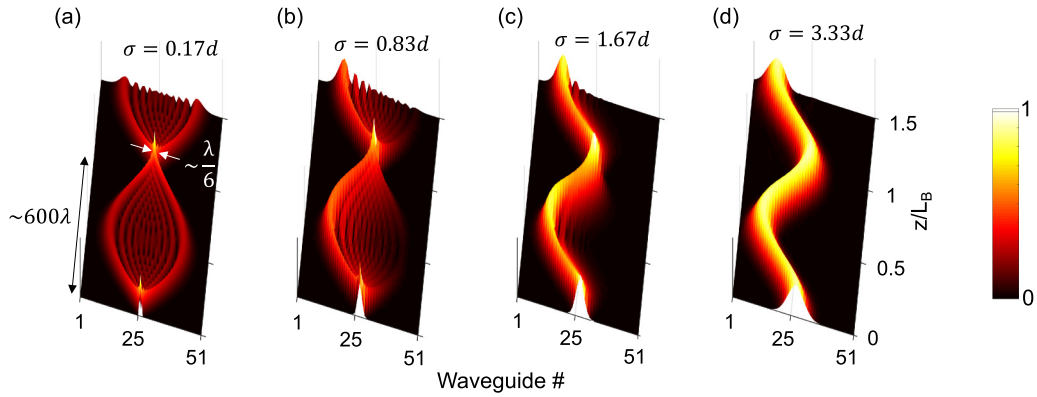

FIG. 3. (a)–(d) Bloch oscillations in a waveguide array with a linear spacing of the propagation constant $\Delta\beta$, for a Gaussian source width $\sigma = 0.17d$, $0.83d$, $1.67d$, and $3.33d$, respectively. The resulting field oscillates periodically with a Bloch period $L_B = 2\pi/\Delta\beta$ (approximately 600λ).

particular example shown in Fig. 3(a), we have $d \approx \lambda/6$ and $L_B \approx 600\lambda$. In a realistic scenario, this focusing mechanism would only be limited by the unavoidable presence of viscothermal losses [41], which might dissipate the acoustic field before it reaches a Bloch period. Subwavelength focusing of optical waves in engineered waveguide arrays has also been discussed in Ref. [42], although using a different physical mechanism.

To characterize experimentally the above described phenomena, we have fabricated a 2-m-long aluminum array composed of $N = 15$ waveguides, as shown in Fig. 4(a). The waveguide width and separation distances are respectively $L = 2.5$ cm and $l = 1$ cm. The H_n and h_n profiles are chosen so that we impose a linear gradient of the propagation constant corresponding to a Bloch period $L_B = 1.5$ m. The numerical values of H_n and h_n are given in Ref. [29]. The acoustic source for exciting the antisymmetric waveguide modes consists of two out-of-phase identical loudspeakers (Clarion SRE 212H) mounted on a screen with two 1-cm-diam holes facing the central waveguide $n = 8$. The acoustic field inside waveguides 3–13 was measured using a 1/4-in. GRAS microphone, placed on the bottom left waveguide corner. The microphone position in the z direction is controlled using a positioning stage with a scanning step of 1 cm. The complex acoustic pressure at the excitation frequency $f = 7260$ Hz is extracted using phase-sensitive detection.

The measured field exhibited an interference pattern along the z direction. We attribute this to several factors, as unwanted reflections at the output section, intrusiveness of the microphone, or the unwanted excitation of symmetric supermodes due to an imperfect antisymmetric excitation with our source. To smooth out this interference we applied a sliding averaging window of ten samples to the measured field. The resulting acoustic field [left panel of Fig. 4(b)] exhibits a breathing motion typical from BOs, with an initial spreading and subsequent refocusing of the wave packet at a distance 1.4 m (≈30λ), very close to the expected Bloch period $L_B =$ 1.5 m. The measured acoustic field is in very good agreement with the numerical simulation [right panel of Fig. 4(b)], where viscothermal losses were included to describe accurately the experimental array. For this, we added an imaginary part to the propagation constants of the supermodes, corresponding to

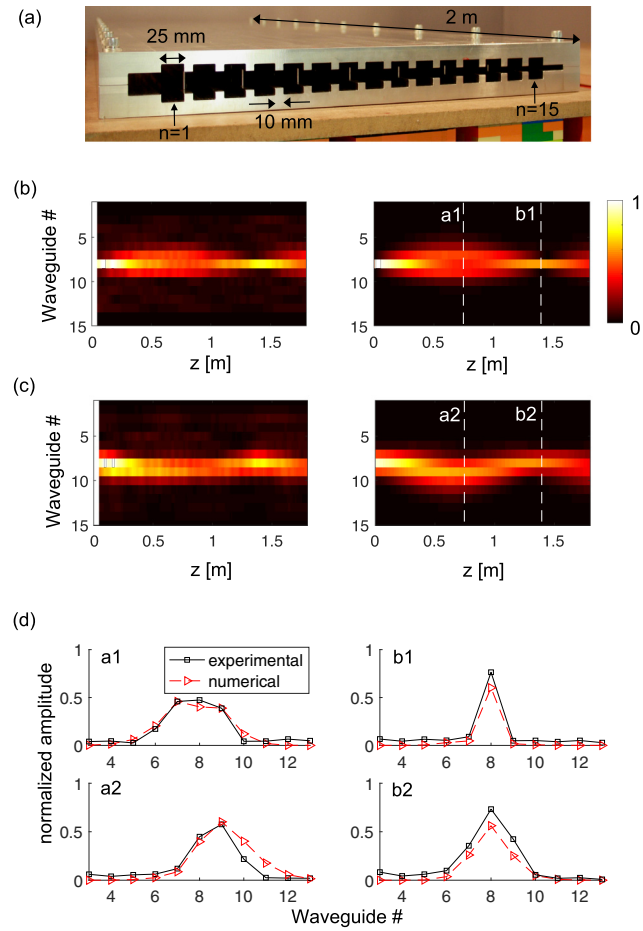

FIG. 4. (a) Picture of the experimental AWA. The AWA consists of 15 waveguides and it is made out of aluminum. The waveguide width is 25 mm and the separation between adjacent waveguides is 10 mm. The varying waveguide height profiles ensures a linear gradient of the AM propagation constant corresponding to $L_B = 1.5$ m. The values of H_n and h_n are given in Ref. [29]. (b) Experimental (left panel) and numerical (right panel) field for a single waveguide excitation. (c) Same as (b) but using a wide excitation covering three waveguides. (d) Cut lines of the experimental and numerical fields at positions $z = 0.75$ m and $z = 1.4$ m, as indicated with dashed lines and labels a1, b1, a2, and b2 in (b) and (c).

the attenuation of the first antisymmetric mode of a waveguide with a rectangular cross section $L \times H_a$, where H_a is the average waveguide height (see Refs. [29,43]). The focal spot is $d = 0.74\lambda$, which was chosen to be larger than in the numerical example in Fig. 3(a) to reduce the intrusiveness of the microphone. However, the important point to realize is that all the energy refocuses within a single lattice site.

Our experimental setup does not allow us to excite multiple waveguides. However, it is possible to construct an approximated response to a broad excitation assuming that the measured Green's function in Fig. 4(b) is independent from the source position (see the discussion in Ref. [29]). Under this assumption, the response of the system to a broad excitation can be obtained as the discrete convolution of the measured Green's function with the desired broad excitation. Figure 4(c) shows the acoustic field for a Gaussian source width $\sigma = 0.9d$, which spans over approximately waveguides 7–9. The experimental result [left panel of Fig. 4(c)] shows the formation of a nondiffractive beam that oscillates in the lateral direction with a period 1.4 m. This result agrees fairly well with the full wave numerical result [right panel of Fig. 4(c)]. For a more quantitative comparison, Fig. 4(d) shows cut lines of the narrow and broad Gaussian excitation response at positions $z = 75$ cm and $z = 140$ cm, as indicated with dashed lines and labels a1, b1, a2, and b2 in Figs. 4(b) and 4(c). These curves corroborate the good agreement between numerical and experimental results, both in the shape and the amplitude of the acoustic field.

In summary, we have investigated discrete diffraction and Bloch oscillations in evanescently coupled acoustic waveguide arrays. Exploiting the phenomenon of Bloch oscillations and through an appropriate choice of the geometrical parameters, we have demonstrated the formation of diffraction-free acoustic beams and subwavelength focusing at distances orders of magnitude larger than the free-space operating wavelength. These results might motivate the design of other types of phononic media (phononic crystals and metamaterials) in which the evanescent coupling between unit cells might lead to unconventional acoustic properties, with potential applications in medical imaging, nondestructive testing, noise control, or audio engineering. In addition, AWAs offer a different perspective on the physics of wave propagation in discrete media.

[1] D. N. Christodoulides, F. Lederer, and Y. Silberberg, Nature (London) **424**, 817 (2003).

[2] I. L. Garanovich, S. Longhi, A. A. Sukhorukov, and Y. S. Kivshar, Phys. Rep. **518**, 1 (2012).

[3] H. S. Eisenberg, Y. Silberberg, R. Morandotti, and J. S. Aitchison, Phys. Rev. Lett. **85**, 1863 (2000).

[4] A. Locatelli, M. Conforti, D. Modotto, and C. D. Angelis, Opt. Lett. **30**, 2894 (2005).

[5] H. S. Eisenberg, Y. Silberberg, R. Morandotti, A. R. Boyd, and J. S. Aitchison, Phys. Rev. Lett. **81**, 3383 (1998).

[6] F. Lederer, G. I. Stegeman, D. N. Christodoulides, G. Assanto, M. Segev, and Y. Silberberg, Phys. Rep. **463**, 1 (2008).

[7] P. Markos and C. M. Soukoulis, *Wave Propagation: From Electrons to Photonic Crystals and Left-Handed Materials* (Princeton University Press, Princeton, NJ, 2008).

[8] T. Pertsch, P. Dannberg, W. Elflein, A. Bräuer, and F. Lederer, Phys. Rev. Lett. **83**, 4752 (1999).

[9] H. B. Perets, Y. Lahini, F. Pozzi, M. Sorel, R. Morandotti, and Y. Silberberg, Phys. Rev. Lett. **100**, 170506 (2008).

[10] A. Schreiber, A. Gábris, P. P. Rohde, K. Laiho, M. Štefaňák, V. Potoček, C. Hamilton, I. Jex, and C. Silberhorn, Science **336**, 55 (2012).

[11] P. M. Preiss, R. Ma, M. E. Tai, A. Lukin, M. Rispoli, P. Zupancic, Y. Lahini, R. Islam, and M. Greiner, Science **347**, 1229 (2015).

[12] J. Feldmann, K. Leo, J. Shah, D. A. B. Miller, J. E. Cunningham, T. Meier, G. von Plessen, A. Schulze, P. Thomas, and S. Schmitt-Rink, Phys. Rev. B **46**, 7252 (1992).

[13] U. Peschel, T. Pertsch, and F. Lederer, Opt. Lett. **23**, 1701 (1998).

[14] A. Block, C. Etrich, T. Limboeck, F. Bleckmann, E. Soergel, C. Rockstuhl, and S. Linden, Nat. Commun. **5**, 3843 (2014).

[15] R. Morandotti, U. Peschel, J. S. Aitchison, H. S. Eisenberg, and Y. Silberberg, Phys. Rev. Lett. **83**, 4756 (1999).

[16] G. Lenz, R. Parker, M. Wanke, and C. de Sterke, Opt. Commun. **218**, 87 (2003).

[17] S. Longhi, M. Marangoni, M. Lobino, R. Ramponi, P. Laporta, E. Cianci, and V. Foglietti, Phys. Rev. Lett. **96**, 243901 (2006).

[18] S. Longhi, Laser Photon. Rev. **3**, 243 (2009).

[19] Y. Ye, M. Ke, J. Feng, M. Wang, C. Qiu, and Z. Liu, J. Phys.: Condens. Matter **27**, 155402 (2015).

[20] N. D. Lanzillotti Kimura, A. Fainstein, and B. Jusserand, Phys. Rev. B **71**, 041305(R) (2005).

[21] H. Sanchis-Alepuz, Y. A. Kosevich, and J. Sánchez-Dehesa, Phys. Rev. Lett. **98**, 134301 (2007).

[22] Z. He, S. Peng, F. Cai, M. Ke, and Z. Liu, Phys. Rev. E **76**, 056605 (2007).

[23] N. D. Lanzillotti-Kimura, A. Fainstein, B. Perrin, B. Jusserand, O. Mauguin, L. Largeau, and A. Lemaître, Phys. Rev. Lett. **104**, 197402 (2010).

[24] M. M. de Lima, Y. A. Kosevich, P. V. Santos, and A. Cantarero, Phys. Rev. Lett. **104**, 165502 (2010).

[25] A. A. Karabutov, Y. A. Kosevich, and O. A. Sapozhnikov, Acoust. Phys. **59**, 137 (2013).

[26] Z. Lazcano and J. Arriaga, Appl. Phys. Lett. **105**, 231901 (2014).

[27] Z. Lazcano, J. Arriaga, and G. N. Aliev, J. Appl. Phys. **115**, 154505 (2014).

[28] Z. Liang, M. Willatzen, and J. Christensen, Phys. Rev. Appl. **4**, 044012 (2015).

[29] See Supplemental Material at http://link.aps.org/supplemental/10.1103/PhysRevB.99.201404 for details on the role and choice of the geometrical parameters (Sec. 1), the numerical modeling using the modal-FE method (Sec. 2), the derivation of the height profiles (Sec. 3), the Wannier-Stark ladders (Sec. 4), and the approximated experimental response to a broad excitation from the measured Green's function (Sec. 5).

[30] A. Pelat, S. Félix, and V. Pagneux, J. Acoust. Soc. Am. **129**, 1240 (2011).
[31] M. Molerón, S. Félix, V. Pagneux, and O. Richoux, J. Appl. Phys. **111**, 114906 (2012)..
[32] M. Molerón, S. Félix, V. Pagneux, and O. Richoux, J. Acoust. Soc. Am. **135**, 74 (2014).
[33] F. Cuevas, S. Curilef, and A. Plastino, Ann. Phys. **326**, 2834 (2011).
[34] S. Hein, W. Koch, and L. Nannen, J. Fluid Mech. **692**, 257 (2012).
[35] V. Pagneux, in *Dynamic Localization Phenomena in Elasticity, Acoustics and Electromagnetism*, edited by R. V. Craster and J. Kaplunov, CISM International Centre for Mechanical Science Courses and Lectures Vol. 547 (Springer, Vienna, 2013).
[36] M. Molerón and C. Daraio, Nat. Commun. **6**, 8037 (2015).
[37] T. Hartmann, F. Keck, H. J. Korsch, and S. Mossmann, New J. Phys. **6**, 2 (2004).
[38] J. B. Pendry, Phys. Rev. Lett. **85**, 3966 (2000).
[39] G. Lerosey, J. de Rosny, A. Tourin, and M. Fink, Science **315**, 1120 (2007).
[40] E. T. F. Rogers, J. Lindberg, T. Roy, S. Savo, J. E. Chad, M. R. Dennis, and N. I. Zheludev, Nat. Mater. **11**, 432 (2012).
[41] M. Molerón, M. Serra-Garcia, and C. Daraio, New J. Phys. **18**, 033003 (2016).
[42] L. Verslegers, P. B. Catrysse, Z. Yu, and S. Fan, Phys. Rev. Lett. **103**, 033902 (2009).
[43] A. M. Bruneau, M. Bruneau, P. Herzog, and J. Kergomard, J. Sound Vib. **119**, 15 (1987).